
OPTICAL FEATURES OF ROTATING QUINTESSENTIAL CHARGED BLACK HOLES IN DE-SITTER SPACETIME

Saeed Ullah Khan^{12*}, Javlon Rayimbaev^{345†}, Furkat Sarikulov^{6‡}, and Ozodbek Abdurakhmonov^{78§}

¹College of Mathematics and Statistics, Shenzhen University, Shenzhen 518060, China

²College of Physics and Optoelectronic Engineering, Shenzhen University, Shenzhen 518060, China

³School of Mathematics and Natural Sciences, New Uzbekistan University, Movarounnahr Str. 1,
Tashkent 100000, Uzbekistan

⁴University of Tashkent for Applied Sciences, Gavhar Str. 1, Tashkent 100149, Uzbekistan

⁵National University of Uzbekistan, Tashkent, Uzbekistan

⁶Ulugh Beg Astronomical Institute, Astronomy Str. 33, Tashkent 100052, Uzbekistan

⁷Institute of Fundamental and Applied Research, National Research University TIAME,
Kori Niyoziy 39, Tashkent 100000, Uzbekistan

⁸PDP University, Yangi Sergeli Str. 12, Tashkent 100022, Uzbekistan

ABSTRACT

One of the most important and actual issues in relativistic astrophysics is testing gravity theories and obtaining constraint values for the parameters of black holes using observational data. In this research, we aimed to explore the optical features of a Kerr–Newman black hole model in the presence of a quintessential field, which may be a candidate for a dark-energy model with a nonzero cosmological constant. First, we obtain the equations of motion for photons using the Hamilton–Jacobi formalism. We also study the horizons and shapes of the apparent regions of the photon region around the said black hole. In various scenarios, we investigate shadows cast by the black hole using celestial coordinates. Furthermore, we analyze the effects of the quintessential field and black hole charge on the shadow radius and distortion. Furthermore, we look into the constraints on the spin and charge of supermassive black holes M87* and Sagittarius A* for different values of the quintessential field using their shadow size measured by the Event Horizon Telescope Collaboration. Finally, we study the effects of the quintessential field, black hole spin and charge on its energy emission rate by Hawking radiation and compare our results with those of the available literature.

Keywords Black holes · Shadow · Photonsphere · Quintessential field · de-sitter spacetime

1 Introduction

According to recent cosmological discoveries, the centers of nearly all galaxies could host supermassive black holes (BHs). Astrophysical evidence, in particular, strongly implies the existence of a BH Sagittarius (Sgr) A* at the center of our galaxy [1]. In 2019, using very long baseline interferometry (VLBI), the Event Horizon Telescope (EHT) project discovered the first shadow picture of a supermassive BH in the center of galaxy M87* [2, 3, 4, 5]. The second picture recently shows how an astrophysical environment, such as the magnetic field, alters the BH image [6]. Despite other evidence, this is the most decisive evidence for the existence of gigantic BHs, leading to new paths for BH research.

The discoveries mentioned above, particularly the EHT project’s visualization of the M87*’s silhouette [2, 7], caught the interest of many researchers to investigate BH shadows [8]. Henceforth, this is a significant area of research to

*drkhan@szu.edu.cn, saeedkhan.u@gmail.com

†javlon@astrin.uz

‡furqatsariquloff@gmail.com

§ozodbekabdu@gmail.com

test general relativity (GR) and modified theories of gravity. Its mathematical aspects [9, 10, 11, 12, 13, 14, 15, 16, 17, 18, 19, 20, 21, 22, 23] established during the years may be investigated using observable data, which can assist us in polishing the mathematical models of these remarkable astrophysical objects. The discovery validates previous mathematical investigations supporting the presence of BHs in our universe and gives a feasible means to check one of GR's core predictions. From ongoing data collection using the Thirty-Meter Telescope [24], the Next Generation Very Large Array [25], and the Black Hole Cam project [26], we anticipate an ideal chance during the upcoming years to gain more insight into the strong gravity regime. To have information on BHs, the study of particle dynamics and the approaches of null geodesics has been an engaging problem in astrophysics [27, 28]. Numerous scholars have looked at the geodesic structure of a BH spacetime [29, 30, 31, 32, 33, 34, 35, 36], as well as compact stars and wormholes [37, 38, 39, 40], as they are of considerable curiosity and have the potential to provide important information while also revealing the effective layout of background geometry.

The photon sphere is a spherical surface that revolves around a BH and contains all conceivable circular orbits of a photon. However, rotating BHs do not have a sphere; rather, they are an area separated from the photon sphere. It describes an area occupied by light-like spherical geodesics. The asymptotically twisted rays of light in one of those light-like spherical geodesics correspond to the outermost edge of the shadow [41]. As a result, the features of the photon regime are critical for studying BH shadows. Bardeen proposed the concept of BHs shadow [42] after deducing that a spacetime BH had $r_{shadow} = 5.2M$ (shadow radius) on the background's light source. Subsequently, many researchers observed that the magnitude of various spinning BH shadows is almost identical to that found earlier [43, 44, 45]. BH seems like a black disk known as a BH silhouette for an outside observer. The shadows of the nonspinning BHs appeared to be a perfect circular disk, whereas the shadows of the revolving BHs deformed in the direction of BH's rotational axis [42, 46]. Recently, Mustafa et al. [47] examined the shadows and weak gravitational lensing by Schwarzschild BH under the influence of the quintessential field.

In the last few decades, analyzing our universe's invisible aspects has piqued numerous researchers' curiosity. Several cosmological datasets revealed that dark energy (DE) is the critical instrument of the accelerating expansion of our universe [48]. Around 68% of our observable universe is compiled of DE [49], which might be described by a repulsive cosmological constant $\Lambda > 0$ or by the quintessence fields [50, 51, 52, 53, 54]. The parameter Λ could be considered homogeneous, with the same value of ($\Lambda \approx 1.3 \times 10^{-56} \text{ cm}^{-2}$) in the space [55]. In addition to the cosmological constant, quintessence is another key component of DE [56]. It is a dynamical and in-homogeneous scalar field with negative pressure, characterized by the expression $\omega = p/\rho$, known as the equation of state, in which p and ρ , respectively, indicate the pressure and energy density of the field. Based on state parameter ω , there exit three cases: corresponding to the phantom energy ($\omega < -1$), the cosmological constant ($\omega = -1$), and the quintessence $\omega \in (-1, -\frac{1}{3})$ [57]. The parameter of state is the most essential characteristic for understanding the concept of DE. As a result, knowing the equation of state is critical for determining DE [58]. The components of DE, namely, the cosmological parameter and/or the quintessential fields of BHs, significantly impact spacetime geometry. As a result, an asymptotic geometry of the spacetime BH takes the form of an asymptotic de-Sitter BH in the existence of a cosmological constant [29, 59]. Consequently, DE or dark matter must be considered in the solutions of BHs.

In recent years, BH, enveloped by the quintessential field, has attracted numerous numbers of scientists. For example, Kiselev [60] postulated the Schwarzschild BH enclosed by a quintessential field, which was later expanded by Toshmatov et al. [61] to the Kerr-like BH; the quasinormal modes, thermodynamics, and phase transition around the Bardeen BH enclosed by quintessence were studied in [62]. Previously, by studying BH shadow in the presence of a cosmological constant and quintessential field, we observed that γ and Λ contribute to the shadow radius, whereas diminishes the distortion effect at higher values [45, 63]. In addition, various authors have hypothesized BHs surrounded by quintessence with a non-vanishing cosmological constant [64, 65].

The key objective of this article is to study the optical features of a Kerr–Newman (KN) BH in the quintessential field with a nonzero cosmological constant (KNdSQ BH). In the following Section 2, we will briefly review the spacetime geometry of a KNdSQ BH. Section 3 explores the characteristics of the photon region around a KNdSQ BH. The fourth Section 4 of our article is devoted to investigating BH shadow and observables. Section 5 of our article deals with the constraints from EHT observations. We investigate the energy emission rates in Section 6. In the last Section 7, we conclude our study with closing remarks.

2 Spacetime metric of the KNdSQ BH

The KN BH provides a more realistic representation of astrophysical BH as most of them, such as spinning and magnetic BHs, are expected to have both angular momentum and charge [66]. It gives an in-depth understanding of the various characteristics BHs may exhibit in the cosmos. The KN BH is a generalization of the Kerr metric, which is extended to include charge, enabling a broader exploration of the BH characteristics and their implications for observational studies.

Moreover, considering the quintessential field, it becomes more interesting and provides a broader examination of BH features. Thus, in the present section, we are interested in investigating the KNdSQ BH, which is the solution of the Einstein–Maxwell equations and has the form in Boyer–Lindquist coordinates [59]

$$ds^2 = \frac{\Delta_\theta \sin^2 \theta}{\rho^2} \left(a \frac{dt}{\Sigma} - (a^2 + r^2) \frac{d\phi}{\Sigma} \right)^2 + \frac{\rho^2}{\Delta_r} dr^2 + \frac{\rho^2}{\Delta_\theta} d\theta^2 - \frac{\Delta_r}{\rho^2} \left(\frac{dt}{\Sigma} - a \sin^2 \theta \frac{d\phi}{\Sigma} \right)^2, \quad (1)$$

with

$$\begin{aligned} \Delta_r &= r^2 - 2Mr + a^2 + Q^2 - \gamma r^{1-3\omega} - \frac{\Lambda}{3} (r^2 + a^2) r^2, \\ \rho^2 &= r^2 + a^2 \cos^2 \theta, \quad \Delta_\theta = 1 + \frac{a^2}{3} \Lambda \cos^2 \theta, \quad \Sigma = 1 + \frac{a^2}{3} \Lambda. \end{aligned}$$

Here M , a , and Q , respectively, stand for BH's mass, spin, and charge. The parameter Λ represents the cosmological constant, whereas γ defines BH's quintessence field's intensity. Moreover, ω describes the equation of state given by $p = \omega\rho$, where ρ and p respectively represent the energy density and pressure of quintessence. By inserting $\gamma = 0$ and replacing Q^2 by q , the metric in Eq. (1) reduces to the braneworld BH with a nonzero cosmological constant [63]; simplifies to the KN case by substituting $\gamma = \Lambda = 0$; reduces to the standard Kerr spacetime with $\gamma = \Lambda = Q = 0$; to the RN BH with $\gamma = \Lambda = a = 0$; and finally to the Schwarzschild BH by setting $\gamma = \Lambda = a = Q = 0$.

Horizons of the above metric (1) are the null hypersurfaces induced by the BH's null geodesics, which can be recovered from the solution of $\Delta_r = 0$, as

$$r^2 - 2Mr + a^2 + Q^2 - \gamma r^{1-3\omega} - \frac{\Lambda}{3} (r^2 + a^2) r^2 = 0. \quad (2)$$

Xu and Wang previously detailed how the parameters γ , a , Q , Λ , and ω define the number of horizons [59]. Furthermore, one should note that its perspectives differ from those of the standard Kerr BH.

By setting $g_{tt} = 0$, the ergosphere may be determined, or equivalent by solving

$$a^2 \sin^2 \theta \Delta_\theta - \Delta_r = 0, \quad (3)$$

it defines the static limit surface (SLS), which is also affected by θ . On letting $\gamma = \Lambda = Q = 0$, the SLS simplifies to the case of standard Kerr BH and accepts the solution

$$r_{SLS\pm} = M \pm \sqrt{M^2 - a^2 \cos^2 \theta}. \quad (4)$$

3 Photon region

This section explores the photon region's characteristics around a KNdSQ BH, with the condition of $p^\mu p_\mu = -m^2$. Henceforth, by applying the technique of separation of variables, the corresponding geodesics motion of metric (1) could be expressed by the Hamilton–Jacobi equation as

$$\mathcal{H} = -\frac{\partial S}{\partial \tau} = \frac{1}{2} g_{\mu\nu} \frac{\partial S}{\partial x^\mu} \frac{\partial S}{\partial x^\nu} = -\frac{1}{2} m^2, \quad (5)$$

in Eq. (5), \mathcal{H} and S , respectively, denote the Hamiltonian and Jacobi action, while m^2 is the rest mass of the particles. But when considering photon orbits, we substitute $m^2 = m_0^2 = 0$. In light of the four-momentum $p_\mu = \partial S / \partial x^\mu$, and by making use of Carter's separability prescription [67], the action could be separated as

$$S = \frac{1}{2} m_0^2 \tau - \mathcal{E} t + L_z \phi + S_r(r) + S_\theta(\theta). \quad (6)$$

The symmetry of spacetime allows us to define the corresponding conserved energy and angular momentum as follows:

$$\mathcal{E} = -p_t = g_{tt} \dot{t} + g_{t\phi} \dot{\phi}, \quad (7)$$

$$\mathcal{L} = p_\phi = g_{t\phi} \dot{t} + g_{\phi\phi} \dot{\phi}. \quad (8)$$

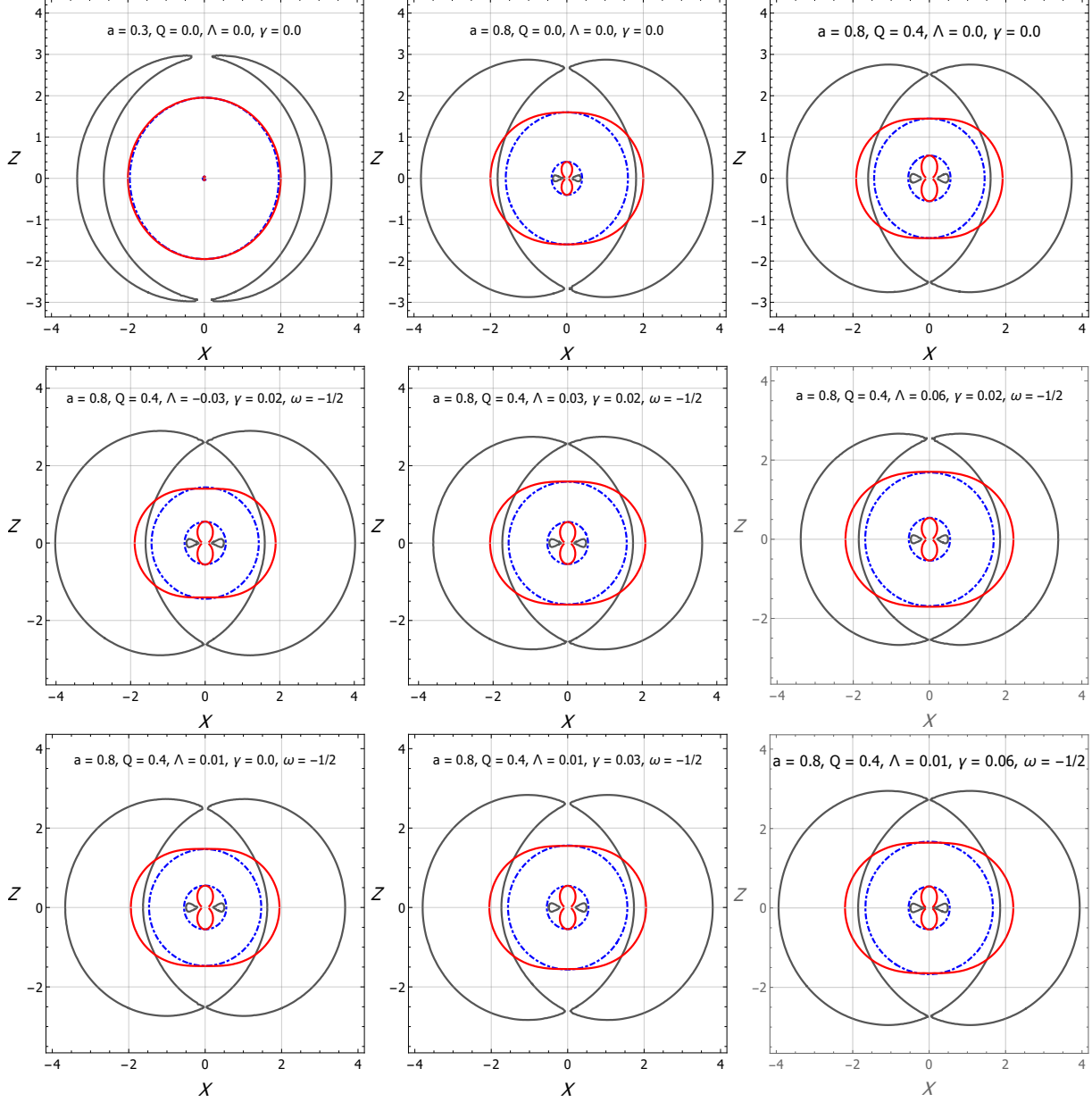


Figure 1: The apparent shapes of the photon region (area between the gray curves on both sides of the origin), Horizons (the inner and outer blue dashed curves, respectively define the Cauchy and event horizon, whereas the inner and outer red curves, respectively represent the inner and outer subsurfaces). Moreover, the area between the event horizon and outer ergosurface is called the ergoregion.

On considering the geometry of the KNdSQ BH, the equations of motion in terms of the four differential equations in the $r - \theta$ plane can be expressed as [68]

$$\rho^2 \frac{dt}{d\tau} = \frac{a}{\Delta_\theta} (\Sigma \mathcal{L} - a \mathcal{E} \sin^2 \theta) + \frac{(a^2 + r^2)}{\Delta_r} ((a^2 + r^2) \mathcal{E} - a \Sigma \mathcal{L}), \quad (9)$$

$$\rho^2 \frac{dr}{d\tau} = \sigma_r \sqrt{\mathcal{R}(r)}, \quad (10)$$

$$\rho^2 \frac{d\theta}{d\tau} = \sigma_\theta \sqrt{\Theta(\theta)}, \quad (11)$$

$$\rho^2 \frac{d\phi}{d\tau} = \frac{\Sigma}{\Delta_\theta} (\Sigma \mathcal{L} \csc^2 \theta - a \mathcal{E}) + \frac{a \Sigma}{\Delta_r} ((a^2 + r^2) \mathcal{E} - a \Sigma \mathcal{L}). \quad (12)$$

In which $\sigma_r = \sigma_\theta = \pm$, with

$$\mathcal{R}(r) = ((a^2 + r^2)\mathcal{E} - a\Sigma\mathcal{L})^2 - \Delta_r((\mathcal{L} - a\mathcal{E})^2 + \mathcal{O}), \quad (13)$$

$$\Theta(\theta) = \mathcal{O}\Delta_\theta - (\mathcal{L}^2 \csc^2 \theta - a^2 \mathcal{E}^2) \cos^2 \theta. \quad (14)$$

In the aforementioned expressions, $\mathcal{O} = \mathcal{K} - (a\mathcal{E} - \mathcal{L})^2$ denotes Carter's constant with \mathcal{K} being the constant of motion. The trajectories of photons around a KNdSQ BH is governed by the above four Eqs. (9)-(12). These trajectories depend mainly on the impact parameters $\xi = \mathcal{L}/\mathcal{E}$ and $\eta = \mathcal{O}/\mathcal{E}^2$ [69]. In principle, photons have three different types of trajectories called scattering, spherical, and plunging orbits; while in terms of ξ and η , the radial Eq. (13) takes the form

$$\mathcal{R}(r) = \frac{1}{\mathcal{E}^2} \left[((a^2 + r^2) - a\Sigma\xi)^2 - \Delta_r((a - \xi)^2 + \eta) \right]. \quad (15)$$

The effective potential on the photon can be straight-forwardly obtained from Eq. (15). Thereafter, the critical and unstable circular orbits could be acquired using the maximum effective potential obeying the following constraints,

$$\mathcal{R}(r) = \frac{\partial \mathcal{R}(r)}{\partial r} \Big|_{r=r_0} = 0. \quad (16)$$

Here r_0 is the radius of photons or unstable circular orbits. Making use of Eq. (16), the celestial coordinates ξ and η can be expressed as

$$\xi = \frac{(a^2 + r^2)\Delta'_r - 4r\Delta_r}{a\Delta'_r\Sigma}, \quad (17)$$

$$\eta = \frac{1}{(a\Delta'_r\Sigma)^2} \left(r^2 (8\Delta_r (2a^2\Sigma^2 + r\Delta'_r) - r^2\Delta_r'^2 - 16\Delta_r^2) - a^2\Delta_r'(1 - \Sigma) (a^2\Delta_r'(1 - \Sigma) + 2r^2\Delta_r' - 8r\Delta_r) \right). \quad (18)$$

It should be noted that the impact parameters listed above are essential, as they determine the boundary of photon orbits. The expression of the photon region in the (r, θ) plane can be obtained by substituting the values of ξ and η (Eqs. (17) and (18)) into $\Theta \geq 0$,

$$\eta \geq \frac{1}{\Delta_\theta} (\xi^2 \csc^2 \theta - a^2) \cos^2 \theta. \quad (19)$$

The graphical behavior of photon region in various cases is presented in Fig. 1. The first row of Fig. 1 provides a comparison between the slowly rotating Kerr (left panel), the fast-rotating Kerr (middle panel), and the Kerr–Newman BH (right panel). Here, one can see that both spin and charge parameters considerably contribute to the area of ergoregion, as well as the photon region backing the previous findings [70, 71]. Our observation summarizes that a fast-rotating charged BH has a greater area of the ergoregion and photon region than the chargeless and slowly rotating BHs. On the other hand, we observed from the second row of Fig. 1 that the negative value of cosmological constant Λ increases the photon region, while $\Lambda > 0$ results in diminishing it, which shows a good agreement with the results of [72]. Moreover, one should note that $\Lambda > 0$ enlarges the event horizon and outer ergosurface (SLS). For the variation of the quintessence parameter γ , we observe that γ contributes to both the inner and outer boundaries of the photon region. However, the inner boundary increases rapidly compared to the outer boundary (see the third row of Fig. 1). Therefore, γ results in a shrinkage of the area of the photon region while contributing to the radii of the event horizon and SLS.

4 BH Shadow

This section is devoted to studying the shadow cast by the KNdSQ BHs. The idea of BH shadow (a dark region in the sky) was initiated by Bardeen in 1973 [42] for the Kerr spacetime. He deduced that BH casts a shadow of about $R_s \simeq 5.2M$ (representing the shadow radius) on a background light source. The boundary of the BH shadow indicates the threshold between escaped and captured photons; in other words, the spherical unstable photon orbits. In literature, such a boundary is known as the “shadow” or “silhouette” of a BH. In principle, the shadow of stationary BHs occurs just like a circular disk, whereas the spin parameter distorts the shadow of spinning BHs. The apparent shape of a BH image can preferably be visualized with the help of celestial coordinates α and β , which, under the assumption of $\Lambda = 0$, could be defined as [44, 69]

$$\alpha = \lim_{r_* \rightarrow \infty} \left(-r_*^2 \sin \theta \frac{d\phi}{dr} \right), \quad (20)$$

$$\beta = \lim_{r_* \rightarrow \infty} \left(r_*^2 \frac{d\theta}{dr} \right). \quad (21)$$

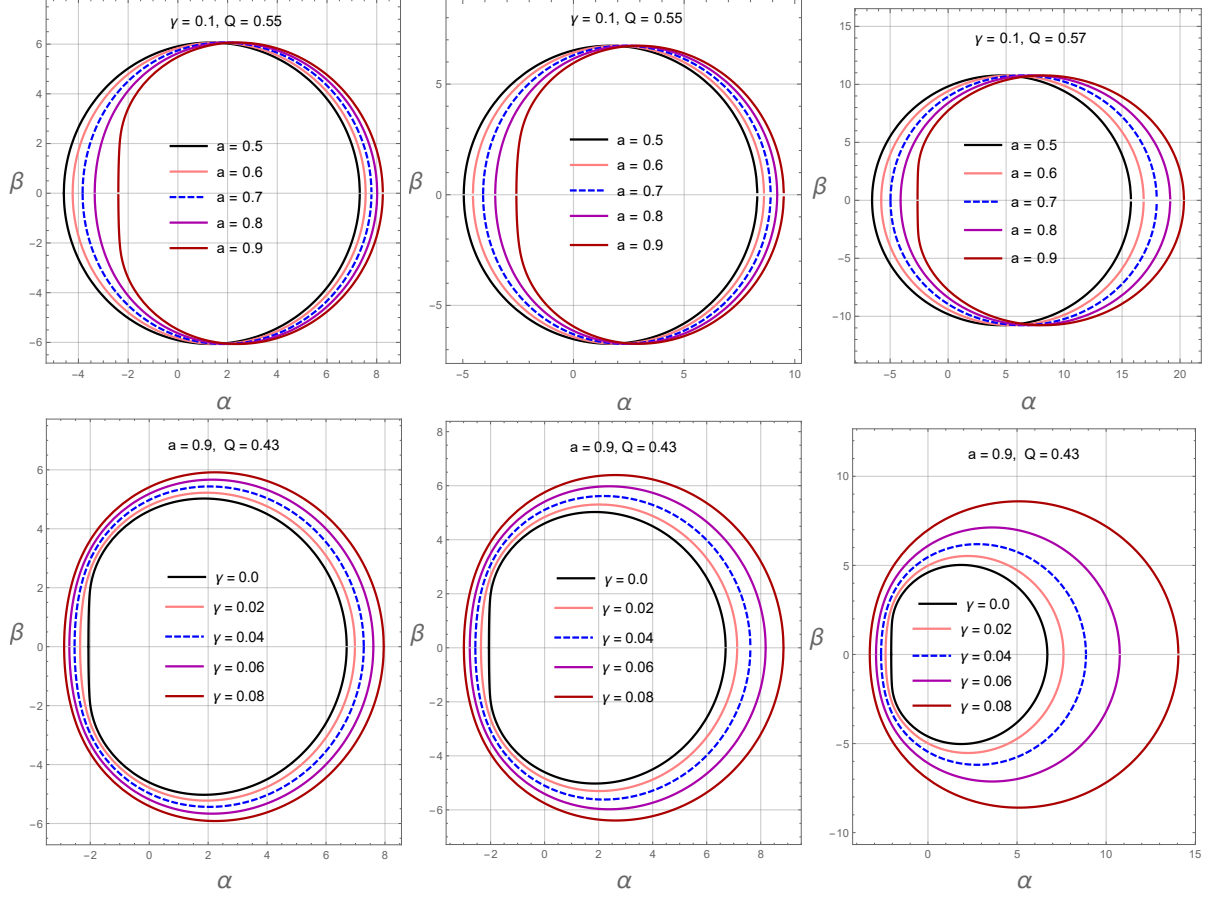


Figure 2: Apparent shape of KNdSQ BH's shadow for the spin parameter (top row), and intensity of the quintessence field γ (bottom row). The left, central and right panels are plotted for $\omega = -2/5$, $\omega = -1/2$ and $\omega = -2/3$, respectively.

In the above expressions, r_* represents the distance between BH and the observer. At the same time, θ denotes the angle of inclination between the observer's line of sight and the spinning axis of BH. By making use of the geodesic equations, the above Eqs. (20) and (21), simplifying to

$$\alpha = -\xi \csc \theta, \quad (22)$$

$$\beta = \pm \sqrt{\eta + a^2 \cos^2 \theta - \xi^2 \cot^2 \theta}. \quad (23)$$

Since BHs shadows are notable on the equatorial plane henceforth, with the substitution of $\theta = \pi/2$, we obtain the following expressions:

$$\alpha = -\xi, \quad (24)$$

$$\beta = \pm \sqrt{\eta}. \quad (25)$$

Leaving $Q = \gamma = 0$ the above expressions (24) and (25) yields

$$\alpha = \frac{a^2(r+M) + r^2(r-3M)}{a(r-M)}, \quad (26)$$

$$\beta = \pm \frac{\sqrt{r^3(4a^2M - r(r-3M)^2)}}{a(r-M)}. \quad (27)$$

The aforementioned expressions, (26) and (27), are precisely the same as those obtained by Hioki & Maeda for the Kerr BH [44].

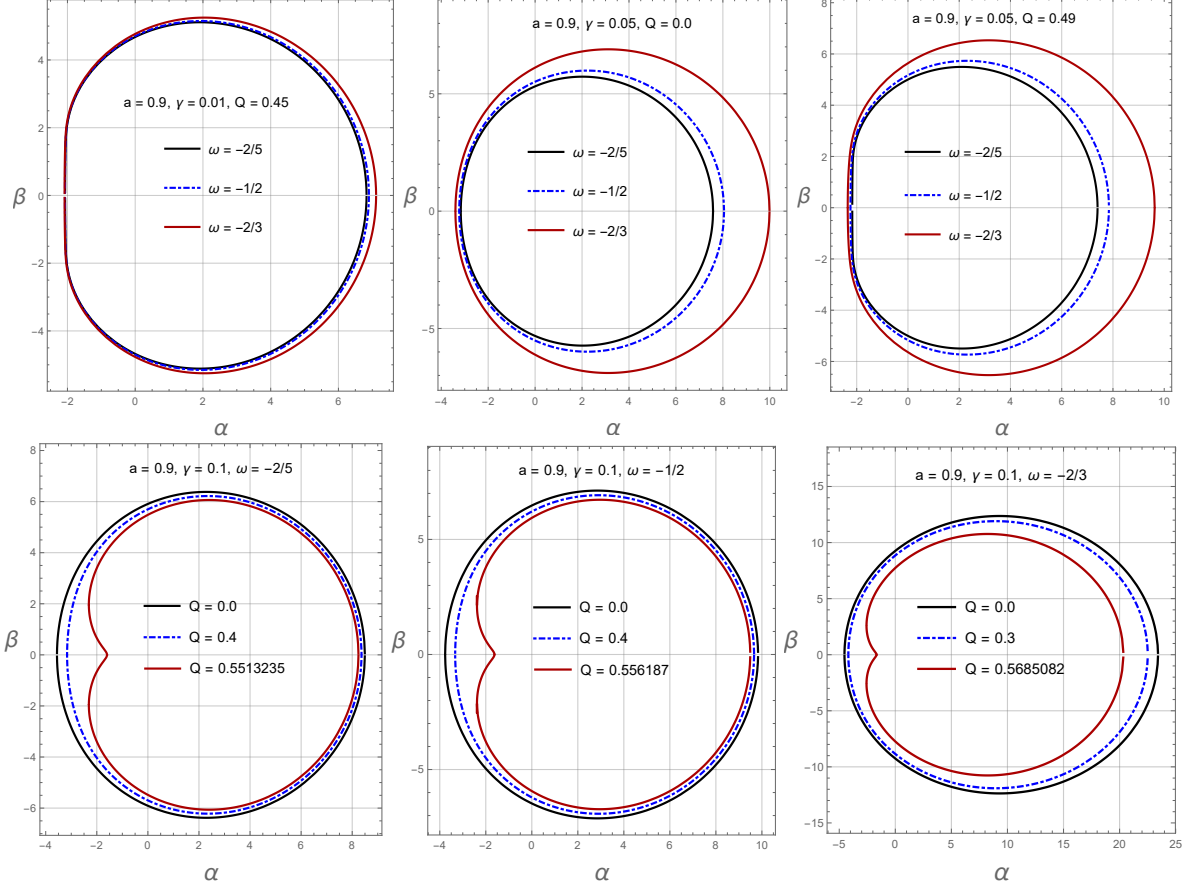


Figure 3: Apparent shape of KNdSQ BH's shadow for the state parameter ω (top row) and BH charge (bottom row).

The visual structure of a KNdSQ BH shadow is illustrated in Figs. 2 and 3. The apparent shape of the BH shadow illustrates that due to the dragging effect, BH spin distorts as well as stretches the shadow it casts in the direction of its axis of rotation, which aligns with the recent findings [73]. In addition, the BH charge contributes to the distortion effect and distorts it considerably in the case of fast rotation (see the first row of Fig. 2). Moreover, the shadow of Kerr BHs appeared wider than that of KN BHs. The quintessence parameter γ elongates the shadow radius while reducing the distortion effect, which becomes negligible at higher values of γ (see the second row of Fig. 2). One should also note that $\gamma > 0$ keeps the shadow away from distortion, and even a smaller value of γ noticeably reduces the distortion effect for details; see Fig. 2 second row.

In addition to other parameters, the absolute value of ω also elongates the BH shadow to the right. The last row of Fig. 3 shows that the BH charge reduces the shadow radius and leads to a more distorted shadow. At the same time, the distortion becomes very intensive at the critical value of the BH charge (for details, see the second row of Fig. 3), which shows great consistency with the results of Ref. [68]. On summarizing the effects of DE energy on BH shadow, we can say that DE expands the apparent shape of BH shadow, while its wideness also depends on the value of ω .

4.1 Observables

To visualize the visible structure of a spinning charged BH in the quintessential field, we explain two observables, namely the silhouette radius R_s and the deformation parameter δ_s , [44]. In fact, the shadow radius R_s can be computed as

$$R_s^2 = \alpha^2 + \beta^2 = \frac{1}{(\gamma + 2(M-r)r^{3\omega} - 3\gamma\omega)^2} \left[(a\gamma(1-3\omega) + 2a(M+r)r^{3\omega})^2 + 2r \left\{ 4r^{6\omega}(-3M^2r + 2MQ^2 + r^3) + 4\gamma r^{3\omega}(3Mr(\omega-1) + Q^2(1-3\omega)) + 3\gamma^2 r(\omega+1)(3\omega-1) \right\} \right]. \quad (28)$$

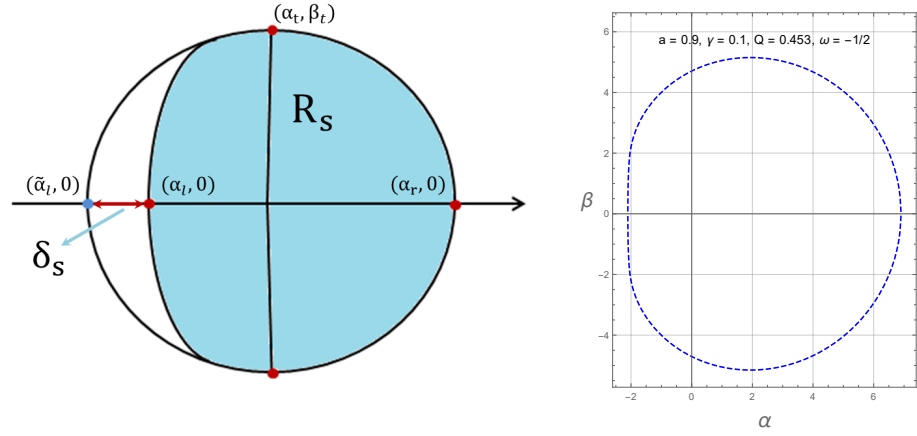


Figure 4: Graphical interpretation of BH shadow and the corresponding reference circle (left), whereas the distorted shadow is cast by a rotating charged BH in the quintessential field (right).

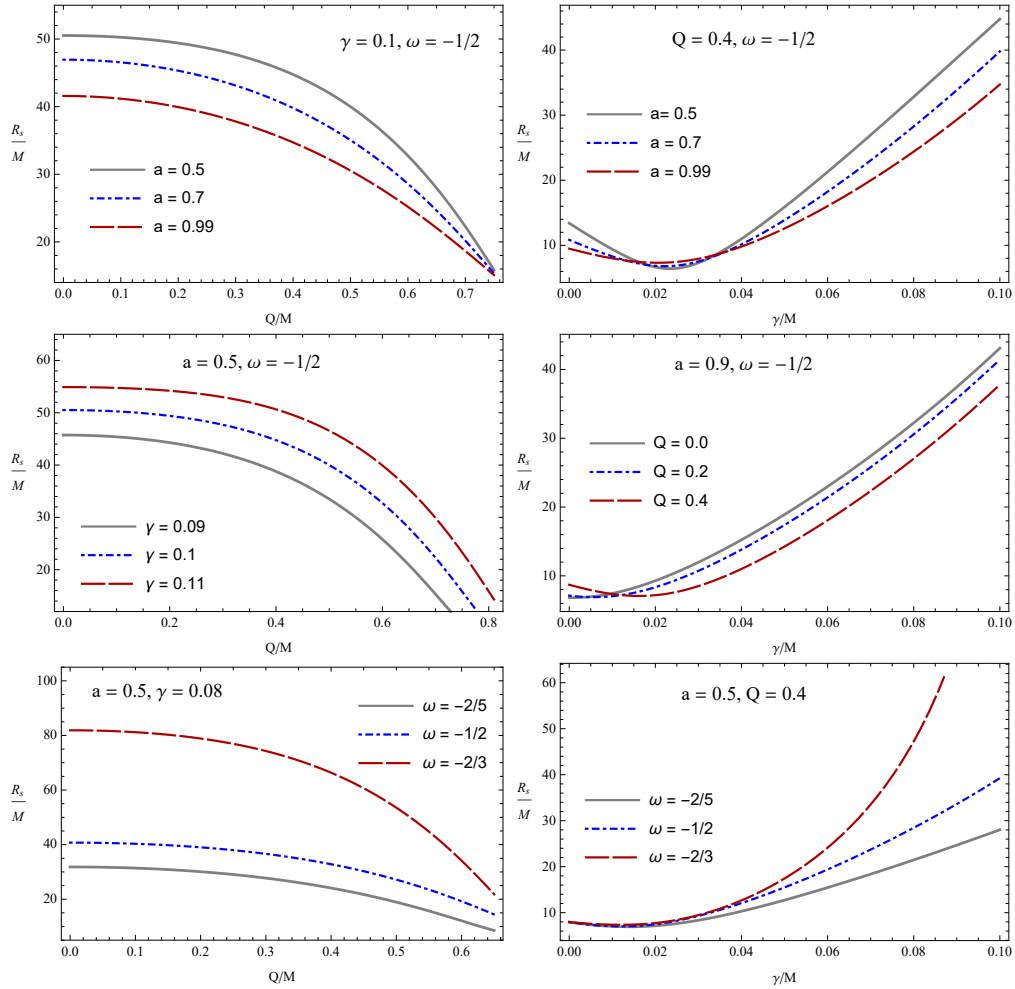


Figure 5: Plots describing the behaviors of Shadow radius R_s .

For non-rotating case, i.e., for $a = 0$, the above expression simplifies to

$$R_s^2 = \frac{1}{(\gamma + 2(M-r)r^{3\omega} - 3\gamma\omega)^2} \left[2r \left\{ 4r^{6\omega}(2MQ^2 + r^3 - 3M^2r) + 4\gamma r^{3\omega}(3Mr(\omega - 1) + Q^2(1 - 3\omega)) + 3\gamma^2 r(\omega + 1)(3\omega - 1) \right\} \right]. \quad (29)$$

While assuming $a = Q = \gamma = 0$, the above expression (28) reduces to the case of Schwarzschild BH and takes the form [74, 75]

$$R_s^2 = \frac{2r^2(r^2 - 3M^2)}{(r - M)^2}. \quad (30)$$

On the other hand, the distortion parameter δ_s defines the deviation of the shadow cast by BHs from an ideal circle,

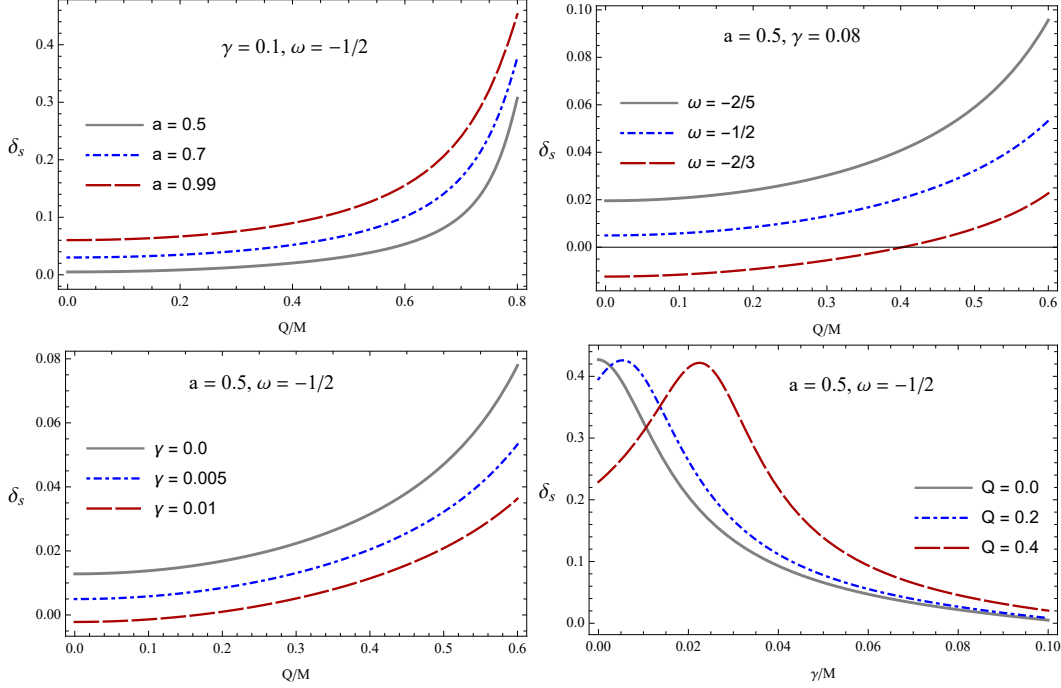


Figure 6: Plots describing the behaviors of deformation parameter δ_s .

which can mathematically be approximated as (see Fig. 4),

$$\delta_s = \frac{|\tilde{\alpha}_l - \alpha_l|}{R_s}. \quad (31)$$

In the above expressions, $(\tilde{\alpha}_l, 0)$ and $(\alpha_l, 0)$ represent the points at which the reference circle and shadow intersect the leftmost α axes.

The shadow radius R_s and the distortion parameter δ_s are plotted in Figs. 5 and 6. The shadow radius is plotted in Fig 5 against charge Q/M (left panels) whereas γ/M (right panels). The graphical description of R_s shows that the quintessence field parameter γ contributes to the shadow radius. On the other hand, BH spin a , charges Q and ω , reduces the shadow radius. Similarly, Fig. 6 illustrates the distortion parameter δ_s . From its graphical interpretation, we observed that γ diminishes the distortion effect in the shadow, whereas the parameters a , Q , and ω contribute to the distortion effects in rotating BHs shadow.

5 Constraints from EHT observations

So far, we have only theoretically investigated the shadow of the KNdSQ BH. Still, a natural question arises: Can the shadow of this BH be compared with shadow images of M87* and Sgr A* obtained by the EHT collaboration? In this section, we aim to get constraints from EHT data. Since many modified/alternative gravity models other than general relativity have been proposed, we should check the viability of all these models by comparing them with our observational data.

To get the constraints, one first needs to define the observable parameters like the radius and the deviation, which we used to describe the size and shape of the BH shadow in the previous section. However, instead of using the Hioki & Maeda method, one can express the area of the shadow with a basic geometric formula in the celestial coordinates and

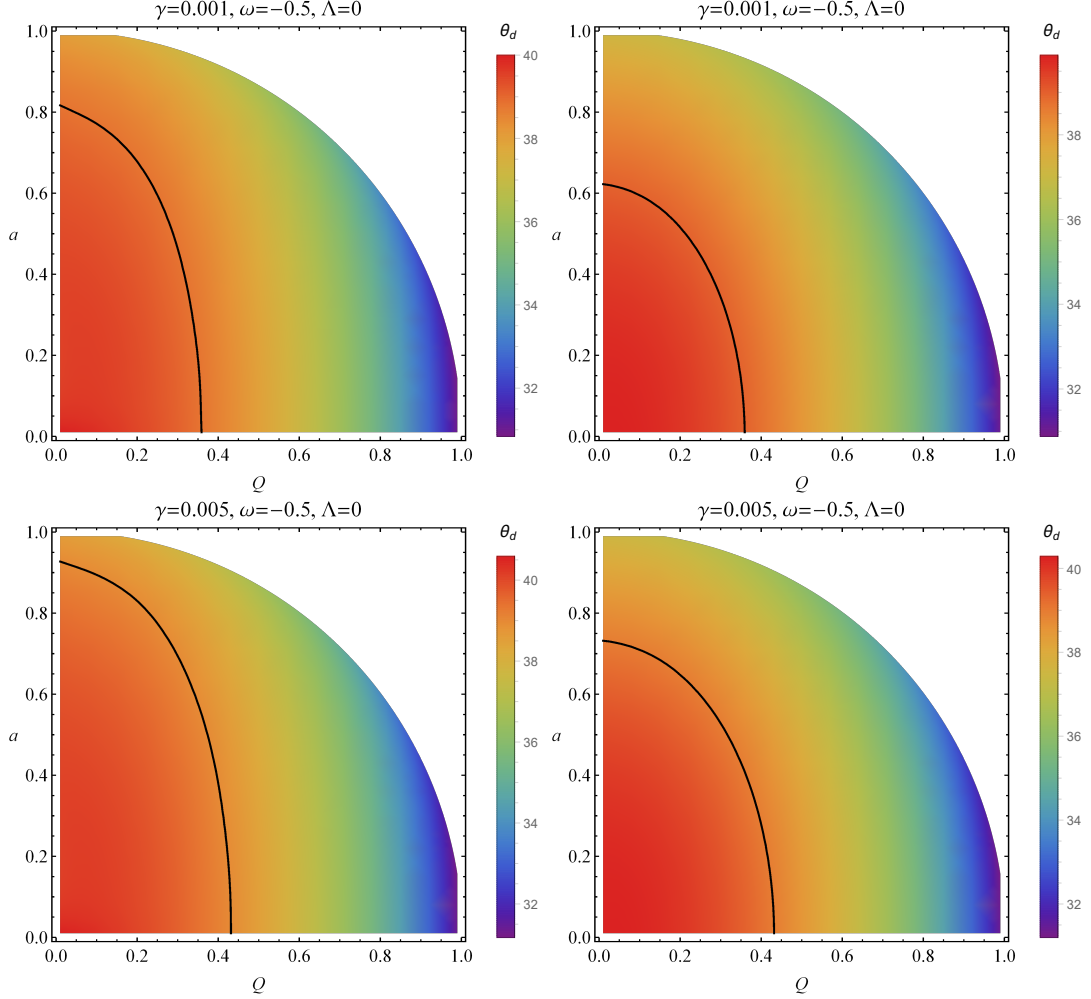


Figure 7: The constraints for M87* for different fixed values of the BH parameters, the inclination angle is 90° for the left panels and 17° for the right panels. The black curves describe the lower borders ($39 \mu as$) of the image size $\theta_d = 42 \pm 3 \mu as$ measured angular diameter of the M87* reported by the EHT.

then define two observables—the area A and the distortion D of the shadow in the following way [76, 77]

$$A = 2 \int_{r_-}^{r_+} \left(\beta(r) \frac{d\alpha(r)}{dr} \right) dr, \quad (32)$$

$$D = \frac{\Delta\alpha}{\Delta\beta}, \quad (33)$$

where r_\pm refers to the prograde and retrograde radii of circular orbits obtained as the roots of equation $\eta_c = 0$, outside the event horizon [78]. The Eqs. (32) and (33) can be used to estimate the BH parameters within the framework of different gravity models by describing the BH parameters as functions of the observable parameters of the shadow [76, 77, 79, 80].

The angular diameter of the shadow image that an observer measures at a distance d from the BH can be expressed as

$$\theta_d = \frac{2R_a}{d}, \quad R_a^2 = \frac{A}{\pi}, \quad (34)$$

where R_a is the areal shadow radius. We have finished with the formulations and can get results by using the information about the shadow of M87* and Sgr A* supermassive BHs reported by the EHT collaboration.

The angular diameter of the image of the BH M87* is $\theta_d = 42 \pm 3 \mu as$ [2]. The mass of M87* and the distance from Earth can be considered as $M = 6.5 \times 10^9 M_\odot$ and $d = 16.8$ Mpc, respectively [81, 82]. For simplicity, in our further calculations, we do not consider the error of the mass and distance measurements of the BHs located at the center of

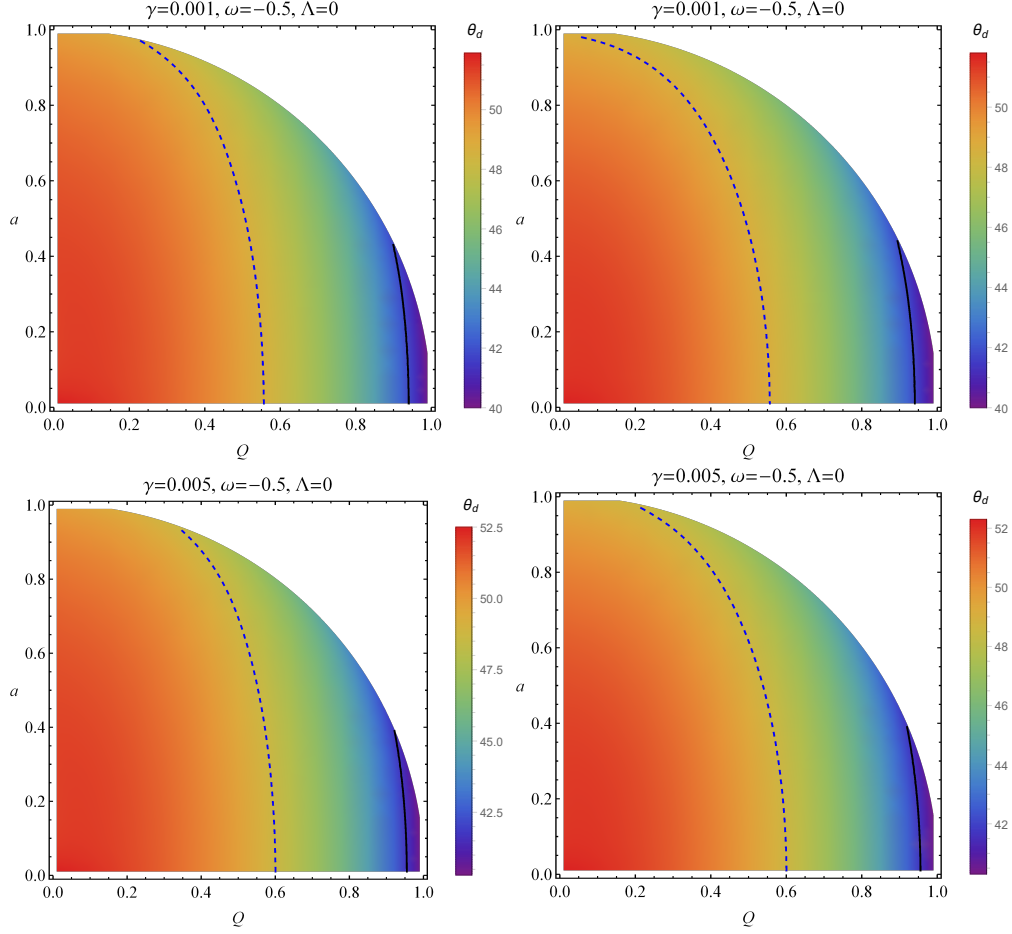


Figure 8: The constraints for Sgr A* are that the angle of inclination is 90° (left) and 50° (right). The black curves correspond to $\theta_d = 41.7 \mu\text{as}$ within the measured angular diameter, $\theta_d = 48.7 \pm 7 \mu\text{as}$ of Sgr A* BH reported by the EHT. The blue dashed curves correspond to $48.7 \mu\text{as}$.

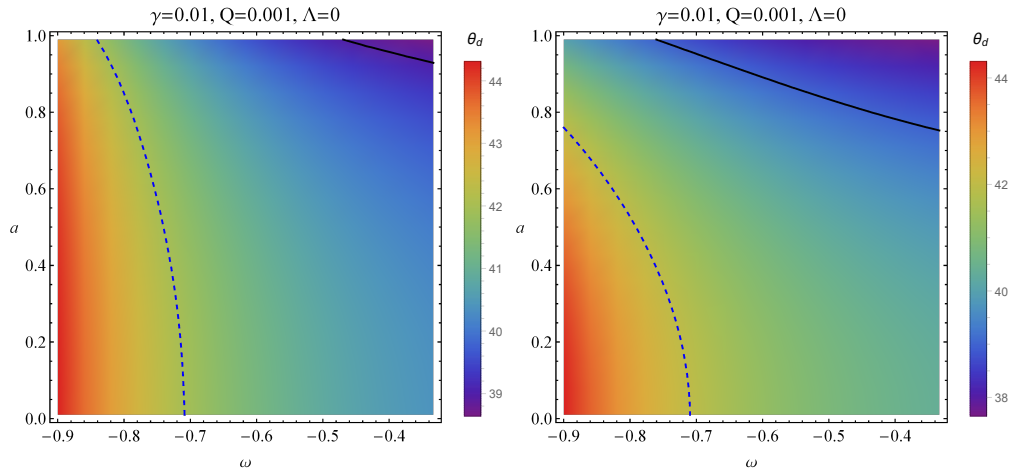


Figure 9: The constraints for M87*: angular diameter observable θ_d for the BH shadows as a function of parameters a and ω at inclinations 90° (left row) and 17° (right row). The black and blue dashed curves correspond to $\theta_d = 39 \mu\text{as}$ and $\theta_d = 42 \mu\text{as}$, respectively.

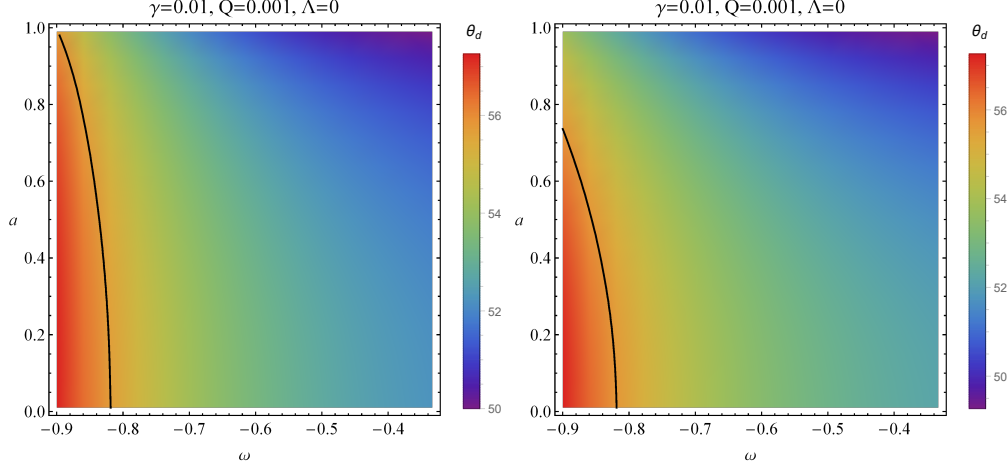


Figure 10: The constraints for Sgr A*: angular diameter observable θ_d for the BH shadows as a function of parameters a and ω at inclinations 90° (left row) and 50° (right row). The black curves correspond to $\theta_d = 55.7 \mu\text{as}$.

M87* and Sgr A*. Using Eq. (34), one can express the angular diameter depending on the BH parameters (including mass) and the inclination angle of the shadow image for an observer located at infinity. Now, we obtain the constraint values for the supermassive BH M87* assuming that the BH is a KNdSQ BH. The results are illustrated in Fig. 7, the angular size of the shadow on the spin and charge parameters for the various values of the other BH parameters at inclination angles 90° and 17° in left and right panels, respectively. Here, the black curves correspond to the lower limit of the measured value of the angular diameter of M87* ($39 \mu\text{as}$). It is observed from the figures that the boundaries of the constraints mainly depend on how the BH parameters change the size of the shadow since the angular diameter is proportional to the area radius of the shadow. For example, the rise of γ causes an increase in the fitted region. Note that change in the inclination angle influences the angular diameter distribution in the a - Q space. Moreover, one can observe from Tables 1 and 2 that a and Q are inversely proportional, whereas a and ω are in direct proportion to each other. In other words, in the case of fast-rotating BHs, the constraint value of charge and ω decreases.

Table 1: Numerical results from the a - Q space constraints at $\gamma = 0.001$, $\omega = -0.5$ and $\Lambda = 0$.

M87*, $39 \mu\text{as}$		Sgr A*, $48.7 \mu\text{as}$	
a	Q	a	Q
0.0	0.3595	0.0	0.5565
0.2	0.3406	0.2	0.5466
0.4	0.2756	0.4	0.5159
0.6	0.0902	0.6	0.4568

Table 2: Numerical results from the a - ω space constraints at $\gamma = 0.01$, $Q = 0.001$ and $\Lambda = 0$.

M87*, $42 \mu\text{as}$		Sgr A*, $55.7 \mu\text{as}$	
a	ω	a	ω
0.0	-0.7094	0.0	-0.8185
0.2	-0.7227	0.2	-0.8251
0.4	-0.7619	0.4	-0.8429
0.6	-0.8268	0.6	-0.8726

Similarly, we calculate the constraints on the supermassive Sgr A* parameters, assuming it is a KNdSQ BH. The angular diameter of the shadow of the Sgr A* is $\theta = 48.7 \pm 7 \mu\text{as}$ [83]. The mass of BH and the distance from the solar system

are $M \simeq 4 \times 10^6 M_\odot$ and $d \simeq 8$ kpc, respectively [84, 85]. Constraints at the angle of inclination 90° (left panels) and 50° (right panels) for Sgr A* are demonstrated in Fig. 8. Here, the black curves correspond to the lower limit ($41.7 \mu\text{as}$) in shadow size, while the blue dashed curves describe its mean value ($48.7 \mu\text{as}$). From all these results, one can get information on which values of the KNdSQ BH parameters can be compared with the Sgr A* or M87* BHs. Just as in the case of M87*, here for Sgr A*, we observed that the same behavior as a and Q shows an inverse proportion, while a and ω are in direct proportion to each other (for details, please see Tables 1 and 2). Surprisingly, in the case of Sgr A*, the constraint values of the charge are much greater, while ω are smaller compared to the supermassive BH M87*.

Furthermore, we considered the charge of BH to be very small and put constraints on the quintessential field parameter. Figs. 9 and 10 show the angular diameter observable θ_l for the BH shadows as a function of parameters a and ω for supermassive BHs M87* and Sgr A*. Moreover, our analysis reveals that the variation in the inclination angle greatly affects the a - ω space distribution of angular diameter.

6 Energy emission

The production and disintegration of enormous particles near the horizon are called energy emissions. The energy emission rate by rotating BHs is an exciting and challenging phenomenon caused by various factors, including Hawking radiation and accretion. According to Stephen Hawking's revolutionary theory, BHs emit radiating heat due to quantum

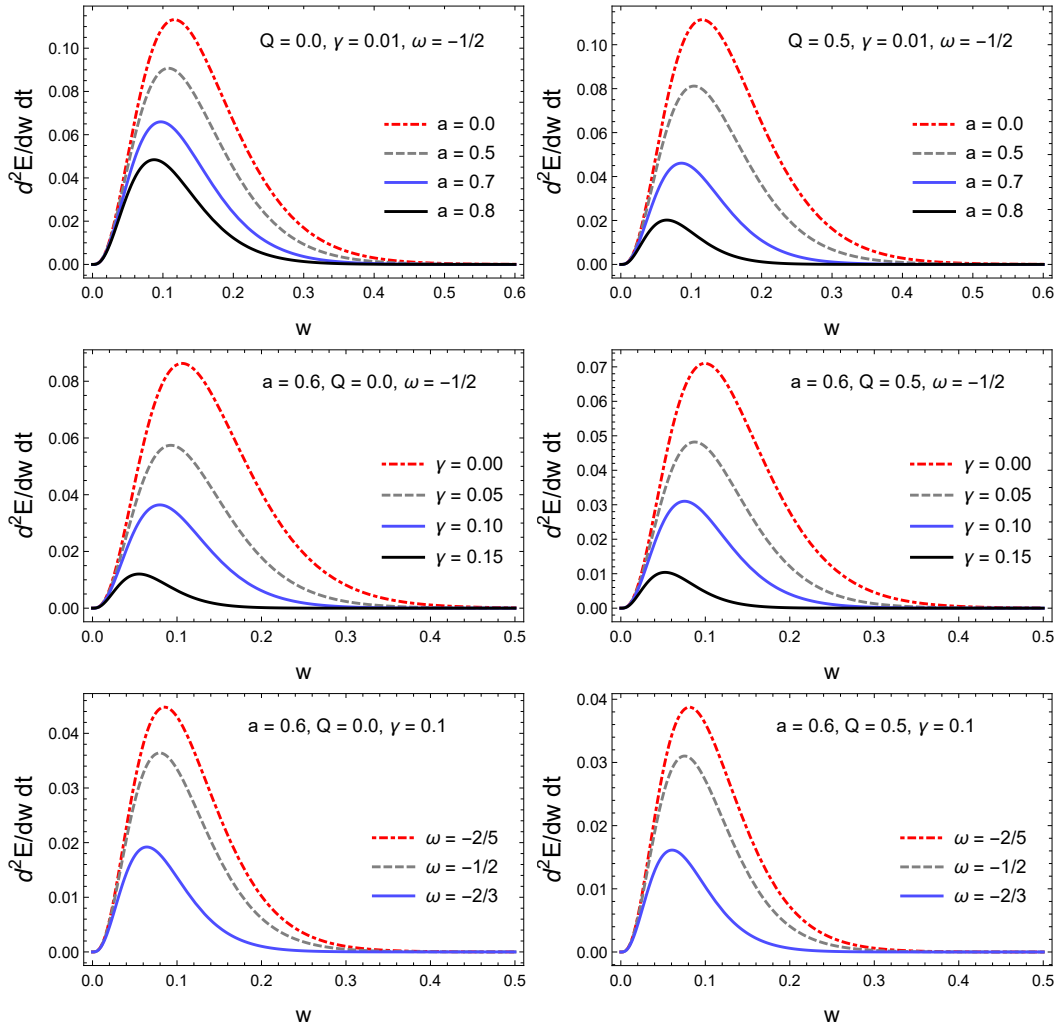


Figure 11: The graphical illustration of energy emission rate along w , in the left column for non-rotating, while in the right column for rotating cases at various discrete values of the parameters Q and γ .

events at their event horizons; hence, they are not entirely black. Hawking radiation is a phenomenon that causes BHs

to lose mass and energy over time. Generally, a small rotating BH emits higher amounts of radiation and loses energy faster than larger ones, as the energy emission rate through Hawking radiation is inversely proportional to the BH's mass. This has a significant impact on BH's lifespan and final results.

According to our assumption, for a distant observer, BH's shadow reaches the high-energy absorption cross-section of the BH [86]. At extreme energies, the absorption cross-section's limiting constant value oscillates around a threshold σ_{ilm} (constant value). The threshold of σ_{ilm} corresponds to the event horizon radius [87]

$$\sigma_{ilm} \approx \pi R_s^2.$$

Thus, the energy emission rate can be computed by making use of the limiting constant value as follows,

$$\frac{d^2 E(w)}{dw dt} = \frac{2\pi^2 R_s^2}{\exp^{w/T-1}}. \quad (35)$$

Here w denotes the photon's frequency, while T is the BH temperature at the event horizon, which can be defined as

$$\begin{aligned} T(r_+) &= \lim_{\theta \rightarrow 0, r \rightarrow r_+} \frac{\partial r \sqrt{g_{tt}}}{2\pi \sqrt{g_{rr}}} \\ &= \frac{1}{4\pi r^{3\omega} (a^2 + r^2)^2} \left[\gamma \left(a^2(3\omega - 1) + r^2(3\omega + 1) \right) - 2r^{3\omega} (a^2 M + r(Q^2 - Mr)) \right]. \end{aligned} \quad (36)$$

Fig. 11 illustrates the behavior of the energy emission rate at various numerical values of the BH parameters. The left panels show the charge-less situation ($Q = 0$), while the right panels show the charged BHs scenario ($Q \neq 0$). We observed that BH charge considerably affects the energy emission rate. Our results confirm that $\gamma > 0$ diminishes the energy emission rate, which is consistent with the theory that larger BHs emit less energy than smaller ones. On the other hand, BH spins a also diminishes the energy emission rate, which is consistent with the findings of [63]. We also discovered that raising the absolute value of the state parameter ω reduces the rate of energy emission (see the third row of Fig. 11). In other words, ω contributes to the BH size; as a result, it results in the decrease of energy emission rate.

7 Conclusion

The key objective of this article is to provide a theoretical analysis of the photon region, BH shadow, and its constraints from the EHT observations. We anticipate our research will be useful for future EHT, James Webb Space Telescope, Square Kilometer Array, and accretion disc observations in various astrophysical environments. Moreover, our findings could provide advancements in the theoretical framework governing quintessential charged BHs. First, we have analyzed the horizon structure of the spacetime geometry around a KNdSQ BH: the horizons and shapes of the apparent regions of the photon region. We discovered that spin and charge parameters significantly impact the area of the ergoregion and the photon region, supporting previous findings [70, 71]. Moreover, our acquired results reveal that fast-rotating charged BHs have greater ergoregion and photon regions than those of chargeless and slowly rotating BHs. Interestingly, we have also observed that $\Lambda < 0$ increases the photon region, while $\Lambda > 0$ diminishes it, showing good agreement with the results of [72]. It is also observed that γ results in shrinking the area of the photon region while contributing to the radii of the event horizon and SLS.

Next, using the Hamilton–Jacobi formalism, we determined the essential equations of motion for photons. The apparent shape of a BH shadow can preferably be visualized with the help of celestial coordinates. Therefore, to explore the shadow cast by KNSdQ BH, we first obtained the corresponding celestial coordinates using null geodesics by following Hioki & Maeda [44]. It has been observed that, due to the effect of the frame-dragging of spacetime, the BH spin stretches its shadow in the direction of the rotational axis. Both charge and spin cause distortion in the BH shadow, consistent with the earlier discovery [68]. Similarly, the quintessence parameter γ elongates the shadow radius, while the quintessence field parameter γ reduces the distortion effect, which becomes negligible at higher values. In addition to other parameters, the absolute value of ω also causes the BH shadow to elongate to the right. In summarizing the effects of DE energy on BH shadow, we can say that DE expands the apparent shape of BH shadow.

We have obtained constraints on BH charge and spin for different values of the quintessential field parameters using the Kumar & Ghosh technique, where we have calculated the area of BH shadow with a basic geometric formula in the celestial coordinates.

We have analyzed the angular size of the shadow on the spin and charge parameters for various choices of the BH's other parameters at inclination angles of 90° and 17° . The boundary values of the constraints are shown to depend on the effect of the BH parameters on the shadow size, which is proportional to the area of the shadow. We have shown

that the growth of γ causes an increase in the fitted region in the a - Q space constraints. Additionally, we assumed that the charge of BH is very small and obtained limitations on the parameters a and ω .

Our analysis of the energy emission rate shows that BH spins a , charge Q , and $\gamma > 0$ diminish the energy emission rate, which is consistent with our previous findings [63], as well as with the theory that states that larger BHs emit less energy as compared to the smaller ones. In addition, we have also found that raising the absolute value of the state parameter ω reduces the rate of energy emission (see the third row of Fig. 11).

Conflicts of Interest

The authors declare that they have no known competing financial interests or personal relationships that could have appeared to influence the work reported in this paper.

References

- [1] Sumarna Haroon, Mubasher Jamil, Kimet Jusufi, Kai Lin, and Robert B. Mann. Shadow and Deflection Angle of Rotating Black Holes in Perfect Fluid Dark Matter with a Cosmological Constant. *Phys. Rev. D*, 99(4):044015, 2019.
- [2] Kazunori Akiyama et al. First M87 Event Horizon Telescope Results. I. The Shadow of the Supermassive Black Hole. *Astrophys. J. Lett.*, 875:L1, 2019.
- [3] Kazunori Akiyama et al. First M87 Event Horizon Telescope Results. II. Array and Instrumentation. *Astrophys. J. Lett.*, 875(1):L2, 2019.
- [4] Kazunori Akiyama et al. First M87 Event Horizon Telescope Results. III. Data Processing and Calibration. *Astrophys. J. Lett.*, 875(1):L3, 2019.
- [5] Kazunori Akiyama et al. First M87 Event Horizon Telescope Results. IV. Imaging the Central Supermassive Black Hole. *Astrophys. J. Lett.*, 875(1):L4, 2019.
- [6] Kazunori Akiyama et al. First M87 Event Horizon Telescope Results. VII. Polarization of the Ring. *Astrophys. J. Lett.*, 910(1):L12, 2021.
- [7] Cosimo Bambi, Katherine Freese, Sunny Vagnozzi, and Luca Visinelli. Testing the rotational nature of the supermassive object M87* from the circularity and size of its first image. *Phys. Rev. D*, 100(4):044057, August 2019.
- [8] Sunny Vagnozzi and Luca Visinelli. Hunting for extra dimensions in the shadow of M87*. *Phys. Rev. D*, 100(2):024020, July 2019.
- [9] J. L. Synge. The Escape of Photons from Gravitationally Intense Stars. *Mon. Not. Roy. Astron. Soc.*, 131(3):463–466, 1966.
- [10] Arne Grenzebach, Volker Perlick, and Claus Lämmerzahl. Photon Regions and Shadows of Kerr-Newman-NUT Black Holes with a Cosmological Constant. *Phys. Rev. D*, 89(12):124004, 2014.
- [11] Ahmadjon Abdujabbarov, Farruh Atamurotov, Naresh Dadhich, Bobomurat Ahmedov, and Zdeněk Stuchlík. Energetics and optical properties of 6-dimensional rotating black hole in pure Gauss–Bonnet gravity. *Eur. Phys. J. C*, 75(8):399, 2015.
- [12] Muhammed Amir and Sushant G. Ghosh. Shapes of rotating nonsingular black hole shadows. *Phys. Rev. D*, 94(2):024054, July 2016.
- [13] Zdeněk Stuchlík, Daniel Charbulák, and Jan Schee. Light escape cones in local reference frames of Kerr–de Sitter black hole spacetimes and related black hole shadows. *Eur. Phys. J. C*, 78(3):180, 2018.
- [14] Ali Övgün, İzzet Sakallı, and Joel Saavedra. Shadow cast and Deflection angle of Kerr-Newman-Kasuya spacetime. *JCAP*, 10:041, 2018.
- [15] Dipanjan Dey, Rajibul Shaikh, and Pankaj S. Joshi. Perihelion precession and shadows near black holes and naked singularities. *Phys. Rev. D*, 102(4):044042, 2020.
- [16] Muhammad Zahid, Saeed Ullah Khan, and Jingli Ren. Shadow cast and center of mass energy in a charged Gauss-Bonnet-AdS black hole. *Chinese Journal of Physics*, 72:575–586, August 2021.
- [17] Mustafa, G. and Hussain, Ibrar and Liu, Wu-Ming. Quasi-periodic oscillations of test particles and red-blue shifts of photons in the charged-Kiselev black hole with cloud of strings. *Chinese Journal of Physics*, 80:148–166, December 2022.

- [18] Atamurotov, Farruh and Hussain, Ibrar and Mustafa, G. and Jusufi, Kimet. Shadow and quasinormal modes of the Kerr-Newman-Kiselev-Letelier black hole. *European Physical Journal C*, 82(9):831, September 2022.
- [19] Allah Ditta, Xia Tiecheng, Saadia Mumtaz, Farruh Atamurotov, G. Mustafa, and Ahmadjon Abdujabbarov. Testing metric-affine gravity using particle dynamics and photon motion. *Physics of the Dark Universe*, 41:101248, August 2023.
- [20] Muhammad Zahid, Javlon Rayimbaev, Furkat Sarikulov, Saeed Ullah Khan, and Jingli Ren. Shadow of rotating and twisting charged black holes with cloud of strings and quintessence. *European Physical Journal C*, 83(9):855, September 2023.
- [21] Atamurotov, Farruh and Hussain, Ibrar and Mustafa, Ghulam and Övgün, Ali. Weak deflection angle and shadow cast by the charged-Kiselev black hole with cloud of strings in plasma. *Chinese Physics C*, 47(2):025102, February 2023.
- [22] Yasir, Muhammad and Xia, Tiecheng and Javed, Faisal and Mustafa, G. Thermal analysis and Joule-Thomson expansion of black hole exhibiting metric-affine gravity. *Chinese Physics C*, 48(1):015103, January 2024.
- [23] Arora, Dhruv and Molla, Niyaz Uddin and Chaudhary, Himanshu and Debnath, Ujjal and Atamurotov, Farruh and Mustafa, G. Exploring tidal force effects and shadow constraints for Schwarzschild-like black hole in Starobinsky-Bel-Robinson gravity. *European Physical Journal C*, 83(11):995, November 2023.
- [24] Gary H Sanders. The thirty meter telescope (tmt): An international observatory. *Journal of Astrophysics and Astronomy*, 34:81–86, 2013.
- [25] A Meredith Hughes, Anthony Beasley, and Christopher Carilli. Next generation very large array: centimeter radio astronomy in the 2020s. *IAU General Assembly*, 29:2255106, 2015.
- [26] C. Goddi et al. BlackHoleCam: Fundamental physics of the galactic center. *Int. J. Mod. Phys. D*, 26(02):1730001, 2016.
- [27] Saeed Ullah Khan and Jingli Ren. Particle dynamics around a dyonic charged black hole. *Chinese Journal of Physics*, 70:55–68, April 2021.
- [28] Saeed Ullah Khan and Zhi-Min Chen. Charged particle dynamics in black hole split monopole magnetosphere. *European Physical Journal C*, 83(8):704, August 2023.
- [29] Z. Stuchlík and S. Hledík. Some properties of the Schwarzschild-de Sitter and Schwarzschild - anti-de Sitter space-times. *Phys. Rev. D*, 60:044006, 1999.
- [30] Arman Tursunov, Zdeněk Stuchlík, and Martin Kološ. Circular orbits and related quasiharmonic oscillatory motion of charged particles around weakly magnetized rotating black holes. *Phys. Rev. D*, 93(8):084012, April 2016.
- [31] Shokhzod Jumaniyozov, Saeed Ullah Khan, Javlon Rayimbaev, Ahmadjon Abdujabbarov, and Bobomurat Ahmedov. Collisions and dynamics of particles with magnetic dipole moment and electric charge near magnetized rotating Kerr black holes. *European Physical Journal C*, 84(3):291, March 2024.
- [32] Javlon Rayimbaev, Marcos Figueroa, Zdeněk Stuchlík, and Bakhtinur Juraev. Test particle orbits around regular black holes in general relativity combined with nonlinear electrodynamics. *Phys. Rev. D*, 101(10):104045, 2020.
- [33] Mustafa, G. and Hussain, Ibrar. Radial and circular motion of photons and test particles in the Schwarzschild black hole with quintessence and string clouds. *European Physical Journal C*, 81(5):419, May 2021.
- [34] Saeed Ullah Khan and Jingli Ren. Circular geodesics in Kerr-Newman-Kasuya black hole. In *American Institute of Physics Conference Series*, volume 2319 of *American Institute of Physics Conference Series*, page 040005, February 2021.
- [35] Saeed Ullah Khan, Uktamjon Uktamov, Javlon Rayimbaev, Ahmadjon Abdujabbarov, Inomjon Ibragimov, and Zhi-Min Chen. Circular orbits and collisions of particles with magnetic dipole moment near magnetized Kerr black holes in modified gravity. *European Physical Journal C*, 84(2):203, February 2024.
- [36] Javed, Faisal and Mumtaz, Saadia and Mustafa, G. and Atamurotov, Farruh and Ghosh, Sushant G. Exploring thin-shell dynamics in regular charged black hole through T-duality. *Chinese Journal of Physics*, 88:55–68, April 2024.
- [37] G. Mustafa, Xia Tie-Cheng, and M. Farasat Shamir. Self-consistent embedded anisotropic quintessence compact stars in Rastall gravity via linear equation of state. *Phys. Scripta*, 96(10):105008, 2021.
- [38] G. Mustafa, Allah Ditta, Saadia Mumtaz, S. K. Maurya, and Değer Sofuoğlu. Study on physical properties and maximum mass limit of Finch–Skea anisotropic model under Karmarkar condition in $f(Q)$ -gravity. *Chinese Journal of Physics*, 88:938–954, April 2024.

- [39] Mustafa, G. and Javed, Faisal and Maurya, S. K. and Ray, Saibal. Possibility of stable thin-shell around wormholes within string cloud and quintessential field via the van der Waals and polytropic EOS. *Chinese Journal of Physics*, 88:32–54, April 2024.
- [40] Kavya, N. S. and Mustafa, G. and Venkatesha, V. and Sahoo, P. K. Exploring wormhole solutions in curvature–matter coupling gravity supported by noncommutative geometry and conformal symmetry. *Chinese Journal of Physics*, 87:751–765, February 2024.
- [41] Yuan Chen, He-Xu Zhang, Tian-Chi Ma, and Jian-Bo Deng. Optical properties of a nonlinear magnetic charged rotating black hole surrounded by quintessence with a cosmological constant. *arXiv e-prints*, page arXiv:2009.03778, September 2020.
- [42] J. M. Bardeen. Timelike and null geodesics in the Kerr metric. *Proceedings, Ecole d’Eté de Physique Théorique: Les Astres Occlus : Les Houches, France, August, 1972, 215-240*, pages 215–240, 1973.
- [43] Rohta Takahashi. Black hole shadows of charged spinning black holes. *Publ. Astron. Soc. Jap.*, 57:273, 2005.
- [44] Kenta Hioki and Kei-ichi Maeda. Measurement of the Kerr Spin Parameter by Observation of a Compact Object’s Shadow. *Phys. Rev. D*, 80:024042, 2009.
- [45] Saeed Ullah Khan and Jingli Ren. Shadow cast by a rotating charged black hole in quintessential dark energy. *Physics of the Dark Universe*, 30:100644, December 2020.
- [46] Volker Perlick, Oleg Yu. Tsupko, and Gennady S. Bisnovatyi-Kogan. Black hole shadow in an expanding universe with a cosmological constant. *Phys. Rev. D*, 97(10):104062, 2018.
- [47] Mustafa, G. and Atamurotov, Farruh and Hussain, Ibrar and Shaymatov, Sanjar and Övgün, Ali. Shadows and gravitational weak lensing by the Schwarzschild black hole in the string cloud background with quintessential field. *Chinese Physics C*, 46(12):125107, December 2022.
- [48] P. J. E. Peebles and Bharat Ratra. The Cosmological Constant and Dark Energy. *Rev. Mod. Phys.*, 75:559–606, 2003.
- [49] Robert Caldwell and Marc Kamionkowski. Dark matter and dark energy. *Nature*, 458:587–589, 2009.
- [50] J. P. Ostriker and Paul J. Steinhardt. The Observational case for a low density universe with a nonzero cosmological constant. *Nature*, 377:600–602, 1995.
- [51] R. R. Caldwell, Rahul Dave, and Paul J. Steinhardt. Cosmological imprint of an energy component with general equation of state. *Phys. Rev. Lett.*, 80:1582–1585, 1998.
- [52] Valerio Faraoni. Inflation and quintessence with nonminimal coupling. *Phys. Rev. D*, 62:023504, 2000.
- [53] C. Adami, F. Durret, L. Guennou, and C. DaRocha. Diffuse light in the young cluster of galaxies CL J1449+0856 at $z=2.07$. *Astron. Astrophys.*, 551:A20, 2013.
- [54] Mustafa, G. and Maurya, S. K. and Ray, Saibal. On the Possibility of Generalized Wormhole Formation in the Galactic Halo Due to Dark Matter Using the Observational Data within the Matter Coupling Gravity Formalism. *The Astrophysical Journal*, 941(2):170, December 2022.
- [55] Z. Stuchlík. Influence of the relict cosmological constant on accretion discs. *Mod. Phys. Lett. A*, 20:561, 2005.
- [56] Edmund J Copeland, Mohammad Sami, and Shinji Tsujikawa. Dynamics of dark energy. *International Journal of Modern Physics D*, 15(11):1753–1935, 2006.
- [57] Paul J. Steinhardt, Limin Wang, and Ivaylo Zlatev. Cosmological tracking solutions. *Phys. Rev. D*, 59(12):123504, June 1999.
- [58] Ji-Ping Dai, Yang Yang, and Jun-Qing Xia. Reconstruction of the Dark Energy Equation of State from the Latest Observations. *The Astrophysical Journal*, 857(1):9, April 2018.
- [59] Zhaoyi Xu and Jiancheng Wang. Kerr-Newman-AdS Black Hole In Quintessential Dark Energy. *Phys. Rev. D*, 95(6):064015, 2017.
- [60] V. V. Kiselev. Quintessence and black holes. *Class. Quant. Grav.*, 20:1187–1198, 2003.
- [61] Bobir Toshmatov, Zdeněk Stuchlík, and Bobomurat Ahmedov. Rotating black hole solutions with quintessential energy. *Eur. Phys. J. Plus*, 132(2):98, 2017.
- [62] Mahamat Saleh, Bouetou Bouetou Thomas, and Timoleon Crepin Kofane. Thermodynamics and Phase Transition from Regular Bardeen Black Hole Surrounded by Quintessence. *Int. J. Theor. Phys.*, 57(9):2640–2647, 2018.
- [63] Saeed Ullah Khan and Jingli Ren. Geodesics and optical properties of a rotating black hole in Randall-Sundrum brane with a cosmological constant. *Chinese Journal of Physics*, 78:141–154, August 2022.

- [64] Mustapha Azreg-Aïnou. Charged de Sitter-like black holes: quintessence-dependent enthalpy and new extreme solutions. *Eur. Phys. J. C*, 75(1):34, 2015.
- [65] Wei Hong, Benrong Mu, and Jun Tao. Thermodynamics and weak cosmic censorship conjecture in the charged RN-AdS black hole surrounded by quintessence under the scalar field. *Nucl. Phys. B*, 949:114826, 2019.
- [66] Hans Stephani, Dietrich Kramer, Malcolm MacCallum, Cornelius Hoenselaers, and Eduard Herlt. *Exact solutions of Einstein's field equations*. Cambridge university press, 2009.
- [67] Brandon Carter. Global structure of the Kerr family of gravitational fields. *Phys. Rev.*, 174:1559–1571, 1968.
- [68] Ernesto F. Eiroa and Carlos M. Sendra. Shadow cast by rotating braneworld black holes with a cosmological constant. *European Physical Journal C*, 78(2):91, February 2018.
- [69] Subrahmanyan Chandrasekhar. *The mathematical theory of black holes*, volume 69. Oxford university press, 1998.
- [70] Saeed Ullah Khan, Misbah Shahzadi, and Jingli Ren. Particle collisions in ergoregion of braneworld Kerr black hole. *Physics of the Dark Universe*, 26:100331, December 2019.
- [71] Mohsen Fathi, Marco Olivares, and José R. Villanueva. Ergosphere, Photon Region Structure, and the Shadow of a Rotating Charged Weyl Black Hole. *Galaxies*, 9(2):43, 2021.
- [72] Yuan Chen, He-Xu Zhang, Tian-Chi Ma, and Jian-Bo Deng. Optical properties of rotating Hayward-de Sitter black hole surrounded by quintessence. *Mod. Phys. Lett. A*, 36(08):2150048, 2021.
- [73] Yi Yang, Dong Liu, Ali Övgün, Gaetano Lambiase, and Zheng-Wen Long. Black hole surrounded by the pseudo-isothermal dark matter halo. *European Physical Journal C*, 84(1):63, January 2024.
- [74] J. L. Synge. The escape of photons from gravitationally intense stars. *Monthly Notices of the Royal Astronomical Society*, 131:463, January 1966.
- [75] Ahmadjon Abdujabbarov, Muhammed Amir, Bobomurat Ahmedov, and Sushant G. Ghosh. Shadow of rotating regular black holes. *Phys. Rev. D*, 93(10):104004, 2016.
- [76] Rahul Kumar and Sushant G. Ghosh. Black Hole Parameter Estimation from Its Shadow. *Astrophys. J.*, 892:78, 2020.
- [77] Misba Afrin, Rahul Kumar, and Sushant G. Ghosh. Parameter estimation of hairy Kerr black holes from its shadow and constraints from M87*. *Mon. Not. Roy. Astron. Soc.*, 504:5927–5940, 2021.
- [78] Edward Teo. Spherical orbits around a Kerr black hole. *Gen. Rel. Grav.*, 53(1):10, 2021.
- [79] Furkat Sarikulov, Farruh Atamurotov, Ahmadjon Abdujabbarov, and Bobomurat Ahmedov. Shadow of the Kerr-like black hole. *Eur. Phys. J. C*, 82(9):771, 2022.
- [80] Misba Afrin, Sunny Vagnozzi, and Sushant G. Ghosh. Tests of Loop Quantum Gravity from the Event Horizon Telescope Results of Sgr A*. *Astrophys. J.*, 944(2):149, 2023.
- [81] Kazunori Akiyama et al. First M87 Event Horizon Telescope Results. V. Physical Origin of the Asymmetric Ring. *Astrophys. J. Lett.*, 875(1):L5, 2019.
- [82] Kazunori Akiyama et al. First M87 Event Horizon Telescope Results. VI. The Shadow and Mass of the Central Black Hole. *Astrophys. J. Lett.*, 875(1):L6, 2019.
- [83] Kazunori Akiyama et al. First Sagittarius A* Event Horizon Telescope Results. I. The Shadow of the Supermassive Black Hole in the Center of the Milky Way. *Astrophys. J. Lett.*, 930(2):L12, 2022.
- [84] Kazunori Akiyama et al. First Sagittarius A* Event Horizon Telescope Results. IV. Variability, Morphology, and Black Hole Mass. *Astrophys. J. Lett.*, 930(2):L15, 2022.
- [85] Kazunori Akiyama et al. First Sagittarius A* Event Horizon Telescope Results. VI. Testing the Black Hole Metric. *Astrophys. J. Lett.*, 930(2):L17, 2022.
- [86] Shao-Wen Wei and Yu-Xiao Liu. Observing the shadow of Einstein-Maxwell-Dilaton-Axion black hole. *JCAP*, 11:063, 2013.
- [87] Faisal Javed, Abdul Basit, Aylin Caliskan, and Ertan Güdekli. Thermal fluctuations, QNMs, and emission energy of charged ADS black hole with nonlinear electrodynamics. *Frontiers in Astronomy and Space Sciences*, 10:1174029, November 2023.